International Journal of Solids and Structures 46 (2009) 2680–2692

Contents lists available at ScienceDirect

International Journal of Solids and Structures

journal homepage: www.elsevier.com/locate/ijsolstr

Cohesive–frictional interface constitutive model

Francesco Parrinello, Boris Failla, Guido Borino *

Università di Palermo, Dipartimento di Ingegneria Strutturale e Geotecnica, Viale delle Scienze, 90128 Palermo, Italy

ARTICLE INFO

Article history:
Received 4 July 2008
Received in revised form 10 February 2009
Available online 20 March 2009

Keywords:
Joined-solids
Interface model
Cohesion
Friction
Damage
Plasticity
FEM

ABSTRACT

In the framework of numerical analysis of joined bodies, the present paper is devoted to the constitutive modeling, via an interface kinematic formulation, of mechanical behaviour of internal adhesive layers. The proposed interface constitutive model couples a cohesive behaviour, based on the damage mechanics theory, with a frictional one, defined in a non-associative plasticity framework. Namely, the interface formulation follows the transition of the adhesive material from the sound elastic condition to the fully cracked one. This formulation is able to model, by means of a specific interpretation of the damage variable and in a relevant mathematical setting, the interface intermediate mechanical properties, during the microcracks spreading process up to the discontinuity surface formation (macrocrack). The constitutive modeling is performed in fully compliance with the thermodynamic principles, in order to ensure the thermodynamic consistency requirement. In the present work, various monotonic and cyclic loading conditions are examined in order to show the main features of the constitutive formulation as well as several significant differences with respect to other existing models. Computational efficiency of the interface constitutive model is tested in a numerical application by FEM resolution strategy approach.

1. Introduction

In the framework of structural analysis a very important and interesting typology of structures is represented by joined solids, which are typically formed by a set of multiple bodies, joined together by means of internal adhesive layers. In this sense, composite laminates, composite structures with inclusions, masonry structures with mortar beds, may be considered as typical joined bodies. The structural response of joined solids, under external loading conditions, is strongly affected by the mechanical behaviour of the internal adhesive layers, where several microstructural failure mechanisms lead to progressive degradation of their mechanical properties, up to complete exhaustion of carrying capacity. Then, an effective constitutive modeling of the adhesive layer behaviour is of primary relevance in the numerical analysis of joined solids structural response. Adhesive layers, due to the fact that their thickness is negligible with respect to sizes of connected bodies, are generally modeled as zero thickness surfaces by means of interface mechanical device, whose internal constitutive law is defined as a relation between traction components and the relevant jump-displacement ones, evaluated at the interface edges.

The microstructural failure mechanisms consist of pointwise phenomena of irreversible deformation and of internal bonds rupture (microcrack), which take place among the constituent elements of adhesive material microstructure (grains of composite structure matrix, aggregates of mortar beds, etc.) and cause pointwise strength reduction and mechanical properties degradation (Carpinteri, 1986; Lemaitre and Chaboche, 1990; Bazant and Planas, 1998). When microcracks spread across the interface microstructure and their spatial diffusion increases, then mechanisms of coalescence and growth of microcracks may begin. Moreover, these mechanisms may evolve, depending on external loading condition, till they produce inside the adhesive layer a discontinuity surface (macrocrack). Macrocraks may close and produce, under compressive loading conditions, the frictional effects related to asperity deformation. Macrocracking phenomena are also followed by a progressive reduction of the structural load carrying capacity and they characterize the structural failure mechanism. For instance, in composite laminates, macrocracks cause delamination phenomena, while, in masonry walls, they cause complete inefficiency of mortar joints. Therefore, it is plain that irreversible microcracking phenomena strongly affect the mechanical structural response and its numerical analysis requires an effective constitutive modeling. Constitutive modeling may be formulated at microscale level, with the drawback of a burdensome computational effort for a multiscale resolution strategy in FEM framework (Liu et al., 2000). Otherwise, it may be formulated at mesoscale level, reproducing the average mechanical behaviour of a material portion, known as representative volume element (RVE) (Lemaitre and Chaboche, 1990), whose size is sufficiently large with respect to the microstructure characteristic dimensions.

Generally, in continuum mechanics, constitutive modeling is devoted to analyse microstructual material properties and to represent them at a specific mesoscale level, in order to catch and to

* Corresponding author.
E-mail addresses: francesco.parrinello@unipa.it (F. Parrinello), bfailla@diseg.unipa.it (B. Failla), borino@unipa.it (G. Borino).

0020-7683/$ - see front matter © 2009 Elsevier Ltd. All rights reserved.
doi:10.1016/j.ijsolstr.2009.02.016

follow the material response in a phenomenological setting. Usually, in the mechanical constitutive modeling via interface formulations, microstructural adhesive material properties are lumped on a zero thickness "Representative Surface Element" (RSE). Interface constitutive relation links traction vector to the displacement jump vector; moreover, some internal variables are involved in order to describe irreversible phenomena. Then, it is possible to define a large variety of mesoscale interface constitutive laws, which model specific sets of microstructural material properties governing the macroscopic phenomena under observation.

In literature, interface constitutive laws have been initially used in the pioneering cohesive-zone models of Dugdale and Barenblatt (Bazant and Planas, 1998), in order to describe the progressive separation process, driven by cohesive traction, in the fracture process zone (FPZ). These cohesive-zone models have been defined in the framework of fracture mechanics, coupled with the damage mechanics and with the plasticity theory. Interface constitutive laws have also been used for modeling fracture propagation phenomena in concrete structures (Hillerborg et al., 1976; Bazant and Oh, 1983; Cedolin et al., 1987). The use of interface models has largely characterized the analysis of composite delamination. In this sense, Allix and Ladeveze have given basic contributions (Allix and Ladeveze, 1992; Allix and Blanchard, 2006), considering that interface constitutive laws allow to model the progressive loss of cohesion between adjacent layers. This constitutive modeling approach is strictly based on the damage mechanics framework, as it can be seen in many considerable contributions on composite delamination matters Corigliano (1993), Mi et al. (1998), Alfano and Crisfield (2001), Qiu et al. (2001), Zou et al. (2003), Point and Sacco (1996). In the latter contributions, plastic and frictional phenomena are neglected. An alternative approach for modeling the progressive decohesion has been developed in the framework of nonassociative softening-plasticity theory. The relevant interface formulations are generally characterized by an initial plastic yielding surface, which models sound material strength and evolves, following a specific hardening/softening law, up to the Coulomb yielding surface, that allows to catch the residual frictional behaviour of the fully cracked material. In the latter theoretical context, in which modeling of elastic properties degradation cannot be performed, interface constitutive models have been defined: for concrete in (Carol et al., 2001) using an hyperbolic initial yield locus; for sands and solids with internal inclusions in Mortara et al. (2002) by means of a Coulomb surface with kinematic and isotropic hardening; in Cocchetti et al. (2002) adopting a piecewise linear yielding surface; for masonry walls in Giambanco and Mroz (2001), Oliveira and Lourenco (2004). Modeling of cohesive damaging behaviour with residual frictional effects has been initially proposed in Tvergaard (1990) for composite laminates, with the feature that frictional behaviour is activated only when complete decohesion is attained. For brittle materials, complete coupling of damaging and frictional effects is developed in Gambarotta and Lagomarsino (1997), Gambarotta (2004). In Alfano and Sacco (2006), Alfano et al. (2006) a new combining method, based on an original mesomechanial assumption, allows to model the transition from pure cohesive damaging behaviour to pure frictional one.

In the present work, an interface constitutive model is developed in order to catch and follow the adhesive material transition from the initial sound state to the final fully cracked one, passing through the spread crack condition, in a thermodynamically consistent framework (Gurtin, 1979; Lemaitre and Chaboche, 1990).

At the initial sound condition, the adhesive material is linearly elastic, while, in the fully cracked state, it is represented by means of a traction-free formulation, with a frictional strength active only under compressive loading conditions. Frictional behaviour is modeled in the framework of nonassociative plasticity theory. The material transition phase is modeled, as proposed in (Alfano and Sacco, 2006), on the basis of damage mechanics theory by a particular and meaningful interpretation, at mesoscale level, of the damage variable, which is the microcracks fraction area of RSE. Damage assumes the role of a mesoscale parameter, able to define the RSE mechanical transition from the sound condition to the completely damaged one (macrocrack formation). From a constitutive point of view, in the transition state, RSE constitutive laws are given by the superposition of the linear elastic model, in its sound fraction, and the traction-free frictional model, in its fully cracked complementary fraction. In this sense, this work may be considered a further contribution to the modeling of coupled adhesive-frictional behaviour (Tvergaard, 1990; Gambarotta and Lagomarsino, 1997; Gambarotta, 2004; Alfano and Sacco, 2006; Alfano et al., 2006). The original aspect introduced in this paper is a different use of the damage variable for the cohesive–frictional transition, in a full thermodynamic consistency. All the above modeling choices involve not only formal differences, but also significant differences in the interface material response, as actual elastic stiffness degradation and positive dissipation in the damaging phenomenon. The present formulation fixes also some aspects related to dilatancy phenomena and it would be a contribution to clarify some recent interface models in a well established framework.

The paper is organized in five sections; in Section 2, the mechanical aspects, related to the fracturing process of the adhesive material layer, are diffusely discussed, with specific regard both to microscale level characterization and to mesoscale level modeling. Section 3 is devoted to a rigorously analytical explanation of the proposed interface constitutive model and, in this sense, several monotonic and cyclic material loading conditions are exposed and comparisons with existing interface models are reported. In Section 4, the results of numerical applications are compared with the experimental data of Magenes and Calvi (1997). Finally, Section 5 is devoted to some concluding remarks.

2. Adhesive material layer: mechanical aspects of fracturing process

In this Section, transition of the adhesive material behaviour, from the initial sound condition to the fully cracked one, is described at microscale level. The theoretical framework on which the interface mesoscale modeling is based, is described in detail.

2.1. Microscale level analysis

In the initial condition, adhesive material shows a reversible mechanical behaviour, due to the fact that microstructure internal bonds are sound and then they are able to transmit traction in all directions in a reversible deformation regime. The loading carrying capacity of the adhesive material may be considered as unlimited for compressive loads, whereas, with reference to tensile and shear loading conditions, it is characterized by a resistance threshold.

Once the strength threshold is reached, pointwise nonlinear phenomena start to take place in microstructure, namely: irreversible deformations and microcracking. These phenomena cause strength reduction and mechanical properties degradation of the adhesive material, which loses its initial reversible mechanical behaviour and enters a transition phase, where irreversible deformation mechanisms and microcracks spread in material microstructure. When microcrack spread nucleation involves a large neighbouring surface of a point, voids start growing and joining together, up to the formation of macroscopic discontinuity surfaces (macrocracks). Macrocrack surfaces are able to transmit compressive traction, as effect of closing processes, and shear traction, due to frictional effects between discontinuity internal edges, but they

are unable to transmit tensile traction. Macrocrack internal surfaces are also characterized by asperities, which determine several phenomena that are coupled with frictional behaviour: asperities reversible and irreversible deformation, asperities smoothing and breaking. Asperities irreversible deformation may show both in tangential direction and in normal one. The tangential deformation mode is related to the relative sliding between macrocrack edges, whereas the normal deformation mode reveals, under compressive loads, as incomplete re-closing of the macrocrack edges. The last phenomenon, known as dilatancy, is caused by mutually sliding among the asperities and its effect gradually reduces, down to zero, with the decrease of the asperities contact surface and with their smoothing and breaking.

2.2. Mesoscale level constitutive modeling

The interface constitutive modeling, at mesoscale level, may be performed by defining specific external and internal state variables, which represent the material state evolution induced by the described microstructural phenomena, as average values on the representative surface element (RSE).

Interface constitutive models typically link the displacement discontinuity, ideally estimated between the adhesion surfaces of the joined bodies, to the relevant adhesion forces. This link is strictly related to soundness condition of adhesive material; therefore, in order to effectively represent it, the specific adhesive material transition, from the sound condition to the fully cracked one, has to be constitutively modeled, selecting the prevailing microstructural behaviour aspects to be considered and the appropriate internal state variables able to phenomenologically describe them.

The spread microcracking phenomenon is classically modeled in the damage mechanics framework (Lemaitre and Chaboche, 1990) considering the RSE, whose size is assumed sufficiently large compared to the adhesive material inhomogeneities, and defining the RSE average damage variable $\bar{\omega}$ as

$$\bar{\omega} = \frac{\Delta S_c}{\Delta S} \tag{1}$$

where ΔS_c is the area of the microcracked RSE portion and ΔS is RSE area, as shown in Fig. 1.

Two distinct effective traction distributions $\boldsymbol{\tau}_s$ and $\boldsymbol{\tau}_c$ may be, respectively, considered at the sound portion $(1-\bar{\omega})\Delta S$ and at the microcracked one $\bar{\omega}\Delta S$ of the RSE (see Fig. 2), where $\boldsymbol{\tau}_c$ play the role of frictional traction. Analogously, two distinct traction vectors $\mathbf{t}_s$ and $\mathbf{t}_c$, acting on RSE, may be defined as in the following

$$\mathbf{t}_s = \frac{1}{\Delta S}\int_{\Delta S} \boldsymbol{\tau}_s dS = (1-\bar{\omega})\bar{\boldsymbol{\tau}}_s \tag{2}$$

$$\mathbf{t}_c = \frac{1}{\Delta S}\int_{\Delta S} \boldsymbol{\tau}_c dS = \bar{\omega}\bar{\boldsymbol{\tau}}_c \tag{3}$$

where $\bar{\boldsymbol{\tau}}_s$ and $\bar{\boldsymbol{\tau}}_c$ are average traction vectors. As long as the RSE size is much smaller than the main interface size, the average damage $\bar{\omega}$ and the average traction vectors $\bar{\boldsymbol{\tau}}_s$ and $\bar{\boldsymbol{\tau}}_c$ can be approximated to the pointwise variables $\omega(\mathbf{x}), \boldsymbol{t}_s(\mathbf{x}) = (1-\omega)\boldsymbol{\tau}_s$ and $\boldsymbol{t}_c(\mathbf{x}) = \omega\boldsymbol{\tau}_c$. In the latter case, which will be followed in the formulation, neither complex homogenization theories nor nonlocal theory are required.

The damage variable ω measures the areal crack density of the infinitesimal surface element dS. Consistently with the damage mechanics theory, variable ω allows us to define, at the material point (mesoscale level), the extent of the microcracked fraction ωdS and of the sound one $(1-\omega)dS$, as discussed in Section 3 (see Fig. 5a and b). By means of the latter assumption, it is possible to adopt, at the mesoscale level, a specific constitutive law for each fraction. In this sense the proposed formulation is a two-scale interface model.

In the following, a linear elastic law is assumed for the sound fraction, whereas a nonassociative elastic-plastic constitutive relation, with Coulomb yield surface, is assigned to the cracked fraction. As a consequence it is possible to model, over an initial elastic behaviour ($\omega = 0$), the complete transition of the adhesive material from a purely cohesive behaviour to a residual frictional one ($\omega = 1$). The compressive behaviour, without any distinction between the sound fraction and the damaged one, is modeled as linearly elastic.

As a concluding remark, it may be pointed out that damage variable is a mesoscale parameter which, besides representing a

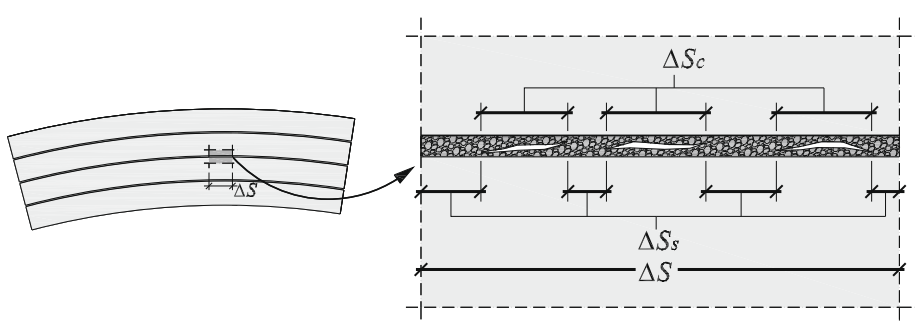

Fig. 1. Mesoscale interpretation of damage variable.

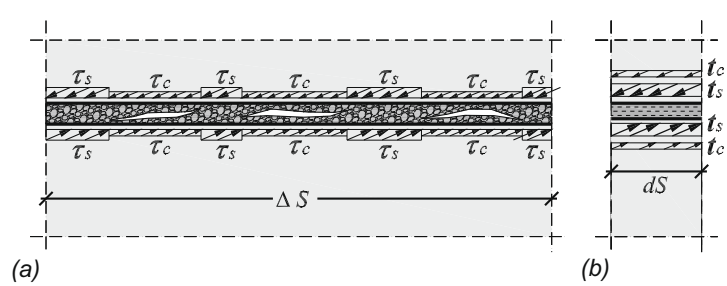

Fig. 2. Mesoscale interpretation of internal static variables: (a) RSE statical configuration; (b) pointwise homogenization.

measure of the spread microcracks area, also governs the progressive transition of the adhesive constitutive model from the initial elastic-cohesive behaviour to the final elastic-frictional one.

3. Constitutive model

In this section, a rigorously analytical explanation of the proposed interface constitutive model, defined in a thermodynamically consistent framework, is reported.

The constitutive model is developed in two-dimensional space, with reference to a zero thickness linear interface, whose kinematical behaviour is represented by the displacement discontinuity across its internal edges. The displacement discontinuity is an interface deformation measure and it may be decomposed in two components: the normal one (Mode I) and the tangential one (Mode II), with reference to the adhesive layer locus. The displacement jump across the interface segment is defined by means of the kinematical variable $[\![\mathbf{u}]\!] = \mathbf{u}^+ - \mathbf{u}^-$, where $\mathbf{u}^+$and $\mathbf{u}^-$are the displacement vectors, respectively, on the positive edge and on the negative one, as shown in Fig. 3. The positive edge is defined with respect to the orientation of the outward normal vector to the interface. The interface equilibrium condition is represented by the following relation $[\![\mathbf{t}]\!] = \mathbf{t}^+ - \mathbf{t}^- = \mathbf{0}$, where $\mathbf{t}^+$ and $\mathbf{t}^-$are the traction vectors, respectively, on the positive edge and on the negative one, as shown in Fig. 4; therefore, it is assumed $\mathbf{t} = \mathbf{t}^+ = \mathbf{t}^-$. These kinematic and static variables are all defined at the macroscale level.

Considering now the mesoscale level, specific constitutive laws must be derived, with the relevant state variables, for the sound fraction $(1-\omega)dS$ and for the spread cracked one ωdS. In the following, the index s is used for the sound fraction variables and index c for the spread cracked fraction ones. The elastic deformation of the adhesive layer, in its sound portion, is measured by the following vector variable

$$\boldsymbol{\delta}_s^e = [\![\mathbf{u}_s]\!] - \boldsymbol{\delta}_s^p \tag{4}$$

where $[\![\mathbf{u}_s]\!]$ is the discontinuity displacement vector and $\boldsymbol{\delta}_s^p$ is the plastic contribution, which represents irreversible deformation phenomena. The kinematical vector variable, assumed to model the reversible behaviour of cracked fraction, represents the asperities elastic deformation, as shown in Fig. 5c, and it is defined as

$$\boldsymbol{\delta}_c^e = [\![\mathbf{u}c]\!] - \boldsymbol{\delta}_c^p - \boldsymbol{\delta}_c^d. \tag{5}$$

where $[\![\mathbf{u}_c]\!]$ is the discontinuity displacement vector, $\boldsymbol{\delta}_c^p$ is its plastic component (Fig. 5d) and $\boldsymbol{\delta}_c^d$ is a detachment displacement (Fig. 5e).

The vector $\boldsymbol{\delta}_c^p$ represents the jump displacement, which is caused by the irreversible sliding of asperities among each others

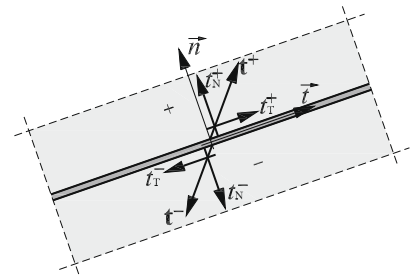

Fig. 4. Interface statics.

and it evolves when the limit frictional strength is attained. Moreover, the frictional behaviour in the microcracked fraction is active only for compressive normal traction and no positive normal traction can be applied, since it would produce loss of contact between the crack edges measured by the detachment displacement $\boldsymbol{\delta}_c^d$.

From a kinematical point of view, with reference to the frictional behaviour of the microcracked fraction, the displacement normal component (denoted by the index N) is characterized by not positive elastic part δ_{cN}^e and by not negative detachment component δ_{cN}^d. Moreover, due to the fact that asperities elastic deformation $\boldsymbol{\delta}_c^e$ and the normal component δ_{cN}^d of the detachment displacement can not be active (i.e. different from zero) at the same time, the following complementarity relations hold

$$\delta_{cN}^e \leqslant 0, \quad \delta_{cN}^d \geqslant 0, \quad \delta_{cN}^e \delta_{cN}^d = 0, \quad \delta_{cT}^e \delta_{cN}^d = 0 \tag{6}$$

and in rate form

$$\dot{\delta}_{cN}^e \delta_{cN}^d = 0, \quad \dot{\delta}_{cT}^e \delta_{cN}^d = 0 \tag{7}$$

$$\delta_{cN}^e \dot{\delta}_{cN}^d = 0, \quad \delta_{cN}^e \dot{\delta}_{cT}^d = 0. \tag{8}$$

The tangential component (denoted by the index T) δ_{cT}^d of the detachment displacement is not subjected to the kinematical constrain of Eq. (6); it means that in a re-closing condition between interface edges, following a detachment path, residual tangential component may be present ($\delta_{cT}^d \neq 0$). Eqs. (6)–(8) state a kinematical constrain between the asperities elastic deformation $\boldsymbol{\delta}_c^e$ and the detachment displacement $\boldsymbol{\delta}_c^d$, which is suitable to control the non-linear behaviour of the microcracked fraction in absence of contact.

The above relations are aimed to model the non-linear problem of plasticity-contact coupling.

In the previous equations, the state variables and the configuration variables, which describe the kinematical behaviour of the sound fraction $(1-\omega)dS$ and of the microcracked one ωdS, have been introduced. The discontinuity displacement vectors $[\![\mathbf{u}_s]\!]$ and

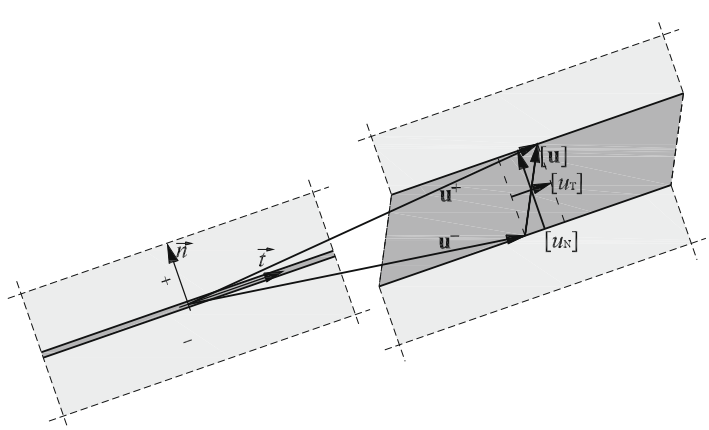

Fig. 3. Interface kinematics.

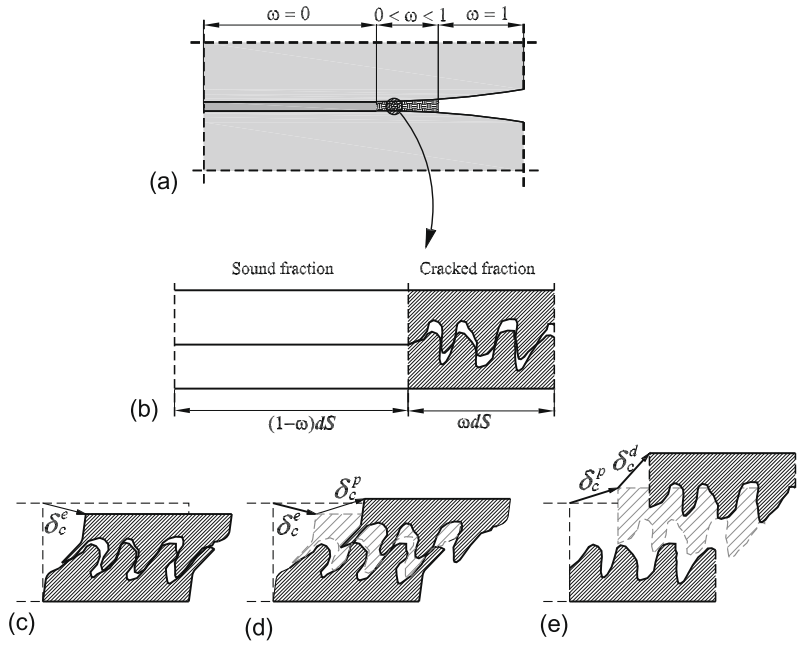

Fig. 5. Macro/meso-scale level representation of cracking phenomenon: (a) macroscale level; (b) mesoscale level; (c) microcracked fraction elastic deformation; (d) microcracked fraction plastic deformation; (e) interface edges detachment.

$[\![\mathbf{u}_c]\!]$ define the deformed configurations of the two fractions. In the ambit of mesoscale constitutive modeling, the deformed configurations of the two fractions are not described independently from each other, as in the composite materials, where the fractions are matrix and fibers and the mesoscale homogeneization procedure provides for a unique pointwise variable to describe the kinematic state. In this sense, the two scales are linked by the following internal compatibility condition.

$$[\![\mathbf{u}]\!] = [\![\mathbf{u}_s]\!] = [\![\mathbf{u}_c]\!]. \tag{9}$$

The stress states of the sound portion and of the microcracked one are, respectively, represented by means of the traction vectors $\mathbf{t}_s$ and $\mathbf{t}_c$, which are the conjugate statical variables of the kinematical elastic strains $\boldsymbol{\delta}_s^e$ and $\boldsymbol{\delta}_c^e$. In order to satisfy the internal equilibrium condition, the Virtual Work Principle is applied in the following form

$$\mathbf{t}^T\delta[\![\mathbf{u}]\!] = \mathbf{t}_s^T\delta[\![\mathbf{u}_s]\!] + \mathbf{t}_c^T\delta[\![\mathbf{u}_c]\!], \tag{10}$$

where $\delta[\![\cdot]\!]$ is a virtual variation; in virtue of Eq. (9), the following equilibrium condition is obtained

$$\mathbf{t} = \mathbf{t}_s + \mathbf{t}_c. \tag{11}$$

The constitutive model is developed in a rigorous thermodynamic framework in the following section.

3.1. Thermodynamically consistent formulation

In order to develop a thermodynamic consistent setting, let Helmholtz free energy density (for unit interface length) be assumed in the following form

$$\begin{aligned}\Psi &= \Psi_{el}(\boldsymbol{\delta}_s^e, \boldsymbol{\delta}_c^e, \omega) + \Psi_{in}(\xi)\\ &= \frac{1}{2}(1-\omega)\boldsymbol{\delta}_s^{eT}\mathbf{K}_s\boldsymbol{\delta}_s^e + \frac{1}{2}\omega\boldsymbol{\delta}_c^{eT}\mathbf{K}_c\boldsymbol{\delta}_c^e + \Psi_{in}(\xi)\end{aligned} \tag{12}$$

where Ψ_{el} and Ψ_{in} are, respectively, the elastic part and the internal one; $\mathbf{K}_s$ and $\mathbf{K}_c$ are diagonal matrices where K_i^s and K_i^c are the elastic moduli, respectively, of the sound fraction and of the microcracked one ($i = N$ normal component, $i = T$ tangential component); ξ is a scalar state internal variable, which governs damage hardening-like, whose physical meaning will be explained later. The second thermodynamic principle, in the form of Clausius–Duhem inequality, reads

$$D = \mathbf{t}^T[\![\dot{\mathbf{u}}]\!] - \dot{\Psi} \geqslant 0, \tag{13}$$

where D is the rate dissipation energy density. Developing the rate form of the Helmholtz free energy of Eqs. (12), (13) becomes

$$D = \mathbf{t}^T[\![\dot{\mathbf{u}}]\!] - \frac{\partial\Psi}{\partial\omega}\dot{\omega} - \frac{\partial\Psi^T}{\partial\boldsymbol{\delta}_s^e}\dot{\boldsymbol{\delta}}_s^e - \frac{\partial\Psi^T}{\partial\boldsymbol{\delta}_c^e}\dot{\boldsymbol{\delta}}_c^e - \frac{\partial\Psi}{\partial\xi}\dot{\xi} \geqslant 0. \tag{14}$$

For an elastic loading step, where $\dot{\omega} = 0, \dot{\xi} = 0, \dot{\boldsymbol{\delta}}_s^p = \mathbf{0}$ and $\dot{\boldsymbol{\delta}}_c^p = \mathbf{0}$, the dissipation D vanishes. Considering the internal compatibility condition (9), it is possible to define the condition

$$\dot{\boldsymbol{\delta}}_s^e = \dot{\boldsymbol{\delta}}_c^e = [\![\dot{\mathbf{u}}]\!]. \tag{15}$$

Substituting last condition in Eq. (14), the following relation holds

$$D = \left(\mathbf{t} - \frac{\partial\Psi}{\partial\boldsymbol{\delta}_s^e} - \frac{\partial\Psi}{\partial\boldsymbol{\delta}_c^e}\right)^T[\![\dot{\mathbf{u}}]\!] = 0, \tag{16}$$

and, because $\mathbf{t}_s$ and $\mathbf{t}_c$ are the conjugated variables, respectively, of the elastic deformations $\boldsymbol{\delta}_s^e$ and $\boldsymbol{\delta}_c^e$, the following positions can be assumed

$$\mathbf{t}_s = \frac{\partial\Psi}{\partial\boldsymbol{\delta}_s^e} = (1-\omega)\mathbf{K}_s\boldsymbol{\delta}_s^e \tag{17}$$

$$\mathbf{t}_c = \frac{\partial\Psi}{\partial\boldsymbol{\delta}_c^e} = \omega\mathbf{K}_c\boldsymbol{\delta}_c^e. \tag{18}$$

Since Eq. (16) has to be verified for any elastic loading step $[\![\dot{\mathbf{u}}]\!]$, the internal equilibrium condition of Eq. (11) is obtained. The overall interface elastic traction–displacement relation is obtained by substituting Eqs. (17) and (18) in Eq. (11)

$$\mathbf{t} = (1-\omega)\mathbf{K}_s\boldsymbol{\delta}_s^e + \omega\mathbf{K}_c\boldsymbol{\delta}_c^e. \tag{19}$$

With reference to the traction vector of the microcracked fraction $\mathbf{t}_c$, from the kinematical constrain Eqs. (6)–(8), it results that

$$t_{cN} \leqslant 0 \tag{20}$$

$$t_{cT} \neq 0 \quad \text{only if} \quad t_{cN} \neq 0. \tag{21}$$

Following a classical thermodynamically consistent approach, the state equations (17) and (18) are assumed to be also valid for inelastic loading steps. In this sense, for a generic inelastic step, Eq. (14) may be written as

$$D = (\mathbf{t}_s + \mathbf{t}_c)^T [\![\dot{\mathbf{u}}]\!] + Y\dot{\omega} - \mathbf{t}_s^T \dot{\boldsymbol{\delta}}_s^e - \mathbf{t}_c^T \dot{\boldsymbol{\delta}}_c^e - \chi\dot{\xi} \geqslant 0, \tag{22}$$

where

$$Y := -\frac{\partial \Psi}{\partial \omega} = \frac{1}{2}\boldsymbol{\delta}_s^{eT}\mathbf{K}_s\boldsymbol{\delta}_s^e - \frac{1}{2}\boldsymbol{\delta}_c^{eT}\mathbf{K}_c\boldsymbol{\delta}_c^e \tag{23}$$

is the energy release rate and

$$\chi(\xi) := \frac{\partial \Psi}{\partial \xi} \tag{24}$$

is the static hardening-like variable.

After some algebra, it is obtained

$$D = \mathbf{t}_s^T \dot{\boldsymbol{\delta}}_s^p + \mathbf{t}_c^T(\dot{\boldsymbol{\delta}}_c^p + \dot{\boldsymbol{\delta}}_c^d) + Y\dot{\omega} - \chi\dot{\xi} \geqslant 0. \tag{25}$$

If the kinematic constrain introduced in Eqs. (6)–(8) is considered, it follows that

$$\mathbf{t}_c^T \dot{\boldsymbol{\delta}}_c^d = 0 \tag{26}$$

and, consequently, the dissipation becomes

$$\begin{aligned} &D = D_p + D_d \geqslant 0, \\ &D_p = \mathbf{t}_s^T \dot{\boldsymbol{\delta}}_s^p + \mathbf{t}_c^T \dot{\boldsymbol{\delta}}_c^p \qquad D_d = Y\dot{\omega} - \chi\dot{\xi}. \end{aligned} \tag{27}$$

Dissipation positiveness is ensured by means of suitable activation criteria, which govern the evolution of plastic and damaging phenomena.

Damage evolution is led by the following yield function

$$\phi_d(Y, \chi) = Y - \chi(\xi) - Y_0 \leqslant 0, \tag{28}$$

with Y_0 assumed as initial yielding threshold.

The internal variable χ governs the growth of the elastic domain and, in this sense, it is called hardening-like variable. The relevant flow rules with the loading-unloading conditions read

$$\begin{aligned} &\dot{\omega} = \frac{\partial \phi_d}{\partial Y}\dot{\lambda}_d = \dot{\lambda}_d, \\ &\dot{\xi} = -\frac{\partial \phi_d}{\partial \chi}\dot{\lambda}_d = \dot{\lambda}_d, \\ &\dot{\lambda}_d \geqslant 0, \quad \phi_d\dot{\lambda}_d = 0, \quad \dot{\phi}_d\dot{\lambda}_d = 0. \end{aligned} \tag{29}$$

It can be shown that damage dissipation results to be always positive for increasing damage

$$D_d = Y_0\dot{\lambda}_d \geqslant 0. \tag{30}$$

Remark 1. The energy release rate Y is the driving thermodynamic force in the damage activation process and it has to satisfy the positiveness requirement. Considering the interface in its initial condition (fully sound material, absence of plastic deformation) and in a compressive stress state, with reference to Eqs. (9) and (23), the following relation holds $\boldsymbol{\delta}_s^e = \boldsymbol{\delta}_c^e$; therefore, the positiveness requirement is fulfilled if and only if the sound elastic moduli are greater than the frictional elastic ones. Moreover, in order to avoid the damage activation in a pure compression stress state, the following positions are assumed

$$\begin{aligned} &K_N^s = K_N^c \\ &K_T^s > K_T^c. \end{aligned} \tag{31}$$

In what follows, in order to give a simpler view of the proposed model, the plastic phenomena in the sound fraction are neglected ($\boldsymbol{\delta}_s^p = \mathbf{0}$), whereas, in microcracked fraction, plastic phenomena evolution is governed by means of the classical Coulomb yield function, generally used for frictional materials,

$$\phi_p = |t_{cT}| + \alpha t_{cN} \leqslant 0. \tag{32}$$

Under the hypothesis of nonassociative plasticity, by means of the following plastic potential

$$\Omega_p = |t_{cT}| + \beta t_{cN}, \tag{33}$$

where α is the frictional coefficient and $\beta = \beta(\delta_{cN}^p)$ is the dilatancy function. The relevant flow rules and loading/unloading conditions are

$$\begin{aligned} &\dot{\delta}_{cT}^p = \frac{\partial \Omega_p}{\partial t_{cT}}\dot{\lambda}_p = \mathrm{sgn}(t_{cT})\dot{\lambda}_p, \\ &\dot{\delta}_{cN}^p = \frac{\partial \Omega_p}{\partial t_{cN}}\dot{\lambda}_p = \beta\dot{\lambda}_p, \\ &\dot{\lambda}_p \geqslant 0, \quad \phi_p\dot{\lambda}_p = 0, \quad \dot{\phi}_p\dot{\lambda}_p = 0. \end{aligned} \tag{34}$$

Dilatancy function is defined as

$$\beta = \beta(\delta_{cN}^p) = \beta_0 H(\bar{\delta} - \delta_{cN}^p), \tag{35}$$

where $\beta_0 < \alpha$ is the dilatancy parameter, $H(\cdot)$ is the Heavyside function and $\bar{\delta}$ is assumed as limit value of dilatancy deformation, which can be considered a parameter related to the characteristic size of asperities. A possible interpretation is that, when dilatancy δ_{cN}^p reaches the limit $\bar{\delta}$, asperities step over each other and the plastic phenomenon only produces tangential sliding between crack surfaces. Plastic dissipation assumes the following form

$$D_p = \mathbf{t}_c^T \dot{\boldsymbol{\delta}}_c^p = (|t_{cT}| + \beta t_{cN})\dot{\lambda}_p > (|t_{cT}| + \alpha t_{cN})\dot{\lambda}_p = 0, \quad \text{for } \dot{\lambda}_p > 0, \tag{36}$$

which shows that positiveness requirement of dissipation is satisfied for plastic phenomena as well as for damaging phenomena. In the present work, the damage hardening-like law is derived assuming a linear softening in the traction-jump displacement law and then, in the internal variable space, by the following constitutive relation

$$\chi(\xi) := \frac{1}{2}K_N^s\bar{u}_e^2\left[\left(\frac{\bar{u}_f}{\bar{u}_f(1-\xi) + \bar{u}_e\xi}\right)^2 - 1\right], \tag{37}$$

where $\bar{u}_e$ and $\bar{u}_f$ are jumps displacement limit values, respectively, at the elastic threshold and at the unitary damage condition, in a pure tensile state. The hardening-like law defined in Eq. (37) produces the following simple mode I and mode II fracture energy

$$G_I = G_{II} = \frac{1}{2}K_N^s\bar{u}_e\bar{u}_f. \tag{38}$$

The mode II fracture energy is related to an interface subjected only to tangential traction, whereas, if the interface is subjected to compressive traction, the frictional dissipation affects the energy required to completely separate the interface edges.

The constitutive parameters governing the proposed model are collected in Table 1.

Table 1
Parameters adopted for the material interface responses.

Sound fraction	Normal elastic stiffness	K_N^s	1500 N/mm^2
	Tangential elastic stiffness	K_T^s	1500 N/mm^2
Cracked fraction	Normal elastic stiffness	K_N^c	1500N/mm^2
	Tangential elastic stiffness	K_T^c	500N/mm^2
	Frictional coefficient	α	0.4877
	Dilatancy coefficient	β	0.2679
	Normal displacement elastic limit	$\bar{u}_e$	0.002 mm
	Normal displacement crack limit	$\bar{u}_f$	0.2 mm
	Dilatancy limit displacement	$\bar{\delta}$	0.05 mm

3.2. Monotonic and cyclic loading material response

In this section the numerical simulations of some different loading paths, which are typically used to validate the interface constitutive model efficiency, are proposed. At this stage, the performed numerical simulations are not devoted to fit any experimental data, but only to show, from a qualitative point of view, the main features of the proposed constitutive model. The constitutive parameters related to the proposed model are described and collected in Table 1.

Fig. 6 shows the results of the numerical simulations of two pure tensile tests (Mode I) performed following, respectively, a monotonic loading path and a cyclic one. The cyclic path is characterized by three loading-unloading paths, in which an increasing opening displacement peak is attained at each cycle, up to full failure. The unloading paths reach compressive stress states. The results point out that the behaviour under tensile stress condition is elastic-damaging, with degradation of initial elastic interface properties and absence of any irreversible deformation phenomenon. Moreover, once compressive stress condition is reached, damaging phenomena do not affect the mechanical response.

Constitutive behaviour of the interface, subjected to a constant normal stress and to an increasing tangential deformation, is shown in Fig. 7a, where five curves are carried out for different values of normal traction component. The curves show an initial linear elastic behaviour up to the damage activation threshold is reached; thereafter, the elastic properties degradation begins and produces a second linear branch, in which the damaged interface behaviour is characterized by coexistence of the cohesive phase and of the elastic-frictional one. When the stress state of the frictional phase attains the Coulomb condition, damage and plastic deformations simultaneously develop; the interface mechanical response follows the descending branch of the stress–strain curves till the interface is completely damaged ($\omega = 1$), whose behaviour is purely frictional, with plastic sliding at constant stress, and is represented by the horizontal segment. Fig. 7b plots dilatancy variable *vs* tangential jump displacement and it shows that dilatancy increases linearly and, once the limit value $\bar{\delta}$ is attained, dilatancy phenomenon exhausts.

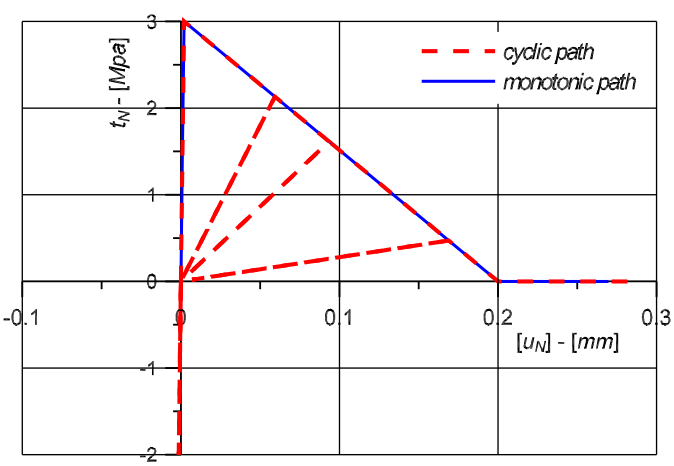

Fig. 6. Cyclic and monotonic tensile tests.

The response of the interface subjected to constant compressive normal component and to cyclic tangential component, which is applied by means of imposed displacements, is reported in Fig. 8a. The curve traction *vs* jump displacement shows the development of hysteretic cycles with progressive elastic properties degradation and with progressive strength reduction down to the residual frictional strength. Fig. 8b plots dilatancy variable evolution compared to imposed tangential displacement.

In Fig. 9 the interface mechanical response to a tangential cyclic load, carried out for three different normal loads, is plotted. The figure shows that the hysteretic cycle amplitude and the relevant dissipated energy are proportional to the applied compressive normal load.

The last loading test is performed for the interface subjected to two tangential loading/unloading cycles, with a constant compressive stress $t_N = -9$ MPa. In order to deeply understand the constitutive model behaviour, the test response is reported in terms of both internal and external traction variables. Fig. 10a shows the tangential stress–strain curves, respectively, for the whole interface, for its sound fraction and for the microcracked one. Fig. 10b shows, in the traction components space, the stress paths followed by the two interface fractions. The branch test is characterized by: initial loading step 1–3, first unloading step 3–4, first reloading step 4–6, second unloading step 6–7, second reloading step 7–8. In detail it may be observed:

- at the steps 1–3, after the initial elastic branch (1–2), damage starts in 2 (Fig. 10a); Fig. 10b shows that, in the elastic branch (1–2), the microcracked stress components do not exist and then, in (2–3), they appear without plastic activation;
- unloading-reloading steps 3-4-3 (Fig. 10a) are elastic with a reduced interface stiffness;
- at steps 3–5 damage increases and at 5 plastic deformation starts in the microcracked fraction, whose stress state reaches Coulomb surface $\phi_p = 0$ (Fig. 10b);

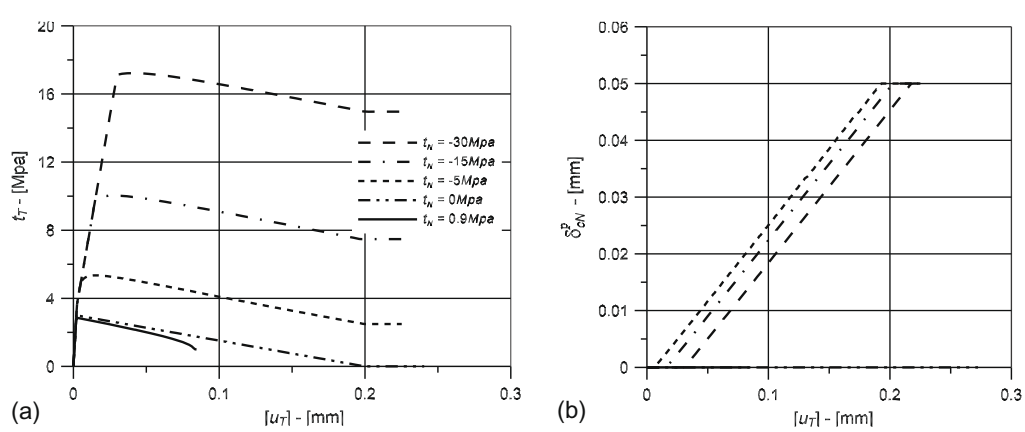

Fig. 7. Shear test for different normal traction values: (a) traction–displacement curves; (b) dilatancy evolution.

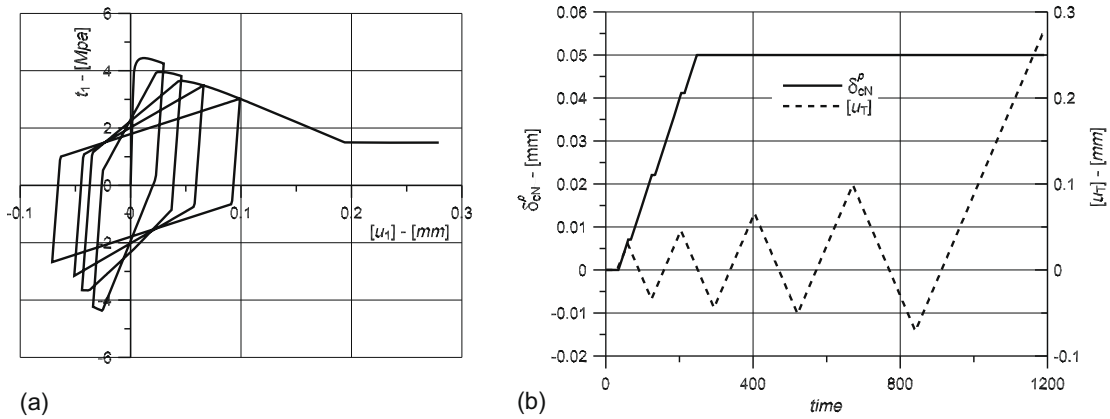

Fig. 8. Cyclic shear test: (a) traction–displacement curve; (b) dilatancy evolution and assigned cyclic tangential displacement evolution.

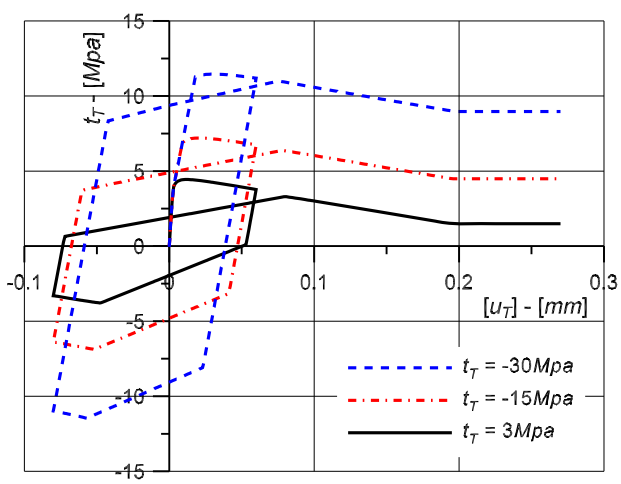

Fig. 9. Cyclic shear tests for different normal traction values.

- reloading step 5–6 is characterized by the coexistence of damage and plastic phenomena;
- unloading step 6–7 shows an initial elastic branch, followed by an elastic–plastic one;
- reloading step 7–8 shows an initial elastic branch, a subsequent elastic–plastic one and, finally, an elastic–plastic-damaging behaviour.

3.3. Comparison with existing models

In this section, the main features of the proposed interface constitutive model as well as fundamental differences, with respect to some of the principal models in literature, are discussed. Elastic–plastic interface constitutive models are widely used in order to simulate the mechanical behaviour of physical joints. The interface constitutive model proposed by (Carol et al., 2001) results to be very interesting and suitable for showing differences between the proposed model and the elastic–plastic interface formulations. The model in (Carol et al., 2001) is characterized by an initial plastic hyperbolic yielding surface, with pure tensile and shear strengths; a specific hardening law leads the transition of the yielding surface up to the classical Coulomb surface, which simulates interface pure frictional behaviour. This condition is reached when interface is fully delaminated. It is obvious that, due to the elastic–plastic approach, the modeling of the interface delamination mechanism is not characterized either by damaging phenomena nor by detachment in opening displacement (Mode I). In fact,

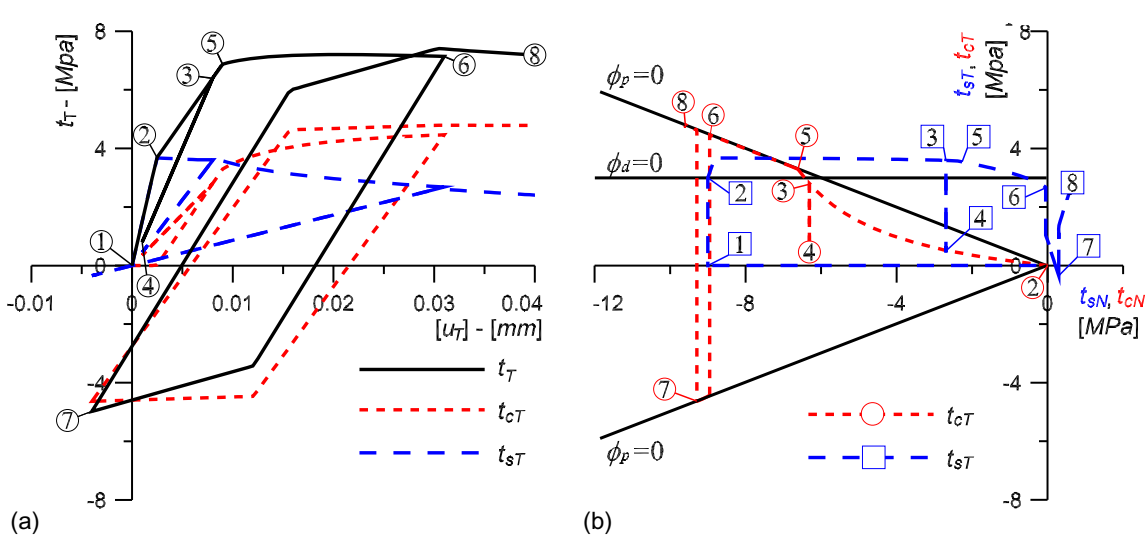

Fig. 10. Cyclic shear test response of interface, sound fraction and cracked fraction: (a) displacement–traction curve; (b) traction components plane.

elastic-plastic models simulate the interface post-delamination opening process by means of plastic strain evolution without energy dissipation; therefore, the fully delaminated interface always shows a plastic opening displacement, without any separation between interface edges. Moreover, in the re-closing step, elastic-plastic models immediately enters the compressive phase, because no detachment displacement characterizes the opening mechanism (Fig. 11a). On the contrary, in the proposed interface model, the post-delamination opening mechanism is governed by the kinematical vector variable $\boldsymbol{\delta}_c^d$, which guarantees that compressive stress state may be present only if the contact condition between interface edges is restored, as shown in Fig. 11b.

Elastic-damaging models are also diffusely used in literature; among them, some approaches are devoted to reproduce interface frictional effects, whereas others ignore this aspect. The interface constitutive model proposed by Alfano and Sacco (2006), Alfano et al. (2006) belongs to the first class and it is based on the same basic feature considered in the proposed work, which regards the specific interpretation of the damage parameter. In fact, in both the interface models, this interpretation consists in considering damage parameter as a physical discriminating term, which is able to distinguish the sound fraction, with a cohesive behaviour, from the fully cracked one, with only a frictional strength. Moreover, the two models present similar damaging and plasticity activation functions. These functions are, qualitatively, represented in the traction components plane of Fig. 12, where surface $\phi_d = 0$ represents the initial damage activation condition (with zero damage variable) and surface $\phi_p = 0$ identifies the final plastic activation condition, when material is fully cracked (damage parameter reaches unit value). Nevertheless, several differences may be noticed between the two models, both from a formal and a substantial point of view, producing significant different results. In the model of Alfano and Sacco (2006), interface equilibrium condition is governed by the following expression $\mathbf{t} = (1-\omega)\mathbf{K}[\![\mathbf{u}]\!] + \omega\mathbf{t}^c$, where $\mathbf{t}^c = \mathbf{K}([\![u]\!] - u^p)$ is the traction vector acting on the cracked fraction; it may be observed that elastic moduli of the two fractions are identical. This condition is substantially different from the one proposed in this work (see Eqs. 11, 17 and 18) and dissimilar results, between the two models, may be pointed out, if the traction path 1-2-3-4, shown in Fig. 12, is followed. It consists in a loading tangential stress branch and in a subsequent unloading one, under a constant compressive normal component; loading branch is extended over the damage activation condition, ensuring that damaging phenomena take place and evolve, but it does not activate frictional plastic deformations. In Alfano and Sacco (2006), loading and unloading phases follow the same path (see Fig. 12), without energy dissipation due to the fact that the sound-cohesive fraction and the cracked-frictional one are characterized by the same elastic tangential moduli. On the contrary, in the present model, damaging effect and relevant energy dissipation are evident. A second difference may be observed with reference to the cyclic test performed in Alfano and Sacco (2006), where damage and plastic deformations are activated at the same time. The same test, using identical constitutive parameters, is analysed by means of the proposed model and the numerical results, compared with the results of Alfano and Sacco (2006) are shown in Fig. 13. The curve related to the proposed model reveals effects of plasticity and of damaging, with the relevant degradation of the elastic properties (strength, stiffness). The curve, which reproduces the results obtained in Alfano and Sacco (2006), identifies a mechanical behaviour which seems to be only affected by plastic deformations, without any elastic stiffness degradation in loading and reloading branches (slope variations are not observable). Therefore, in Alfano and Sacco (2006), damage variable is only used as sound-cracked fractions identification parameter and does not take into account damaging degradation effects and the related damage dissipation.

4. Numerical simulation

The proposed interface constitutive model has been implemented in the FEAP, (Zienkiewicz and Taylor, 2000), finite element code, by developing a six nodes interface element with Gauss numerical integration, for two-dimensional analyses. In FE framework, the analysis of structural problem is performed by means

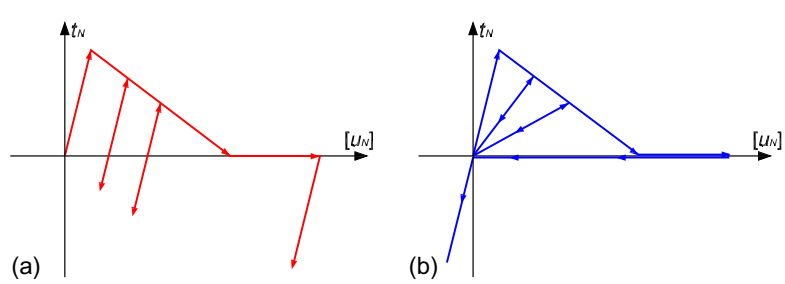

Fig. 11. Models comparison for tensile behaviour: (a) elastic–plastic model. (b) elastic-damaging model.

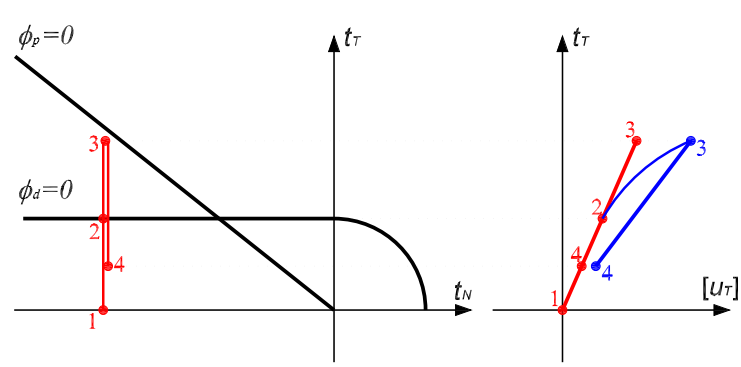

Fig. 12. Models comparison in a loading-unloading path.

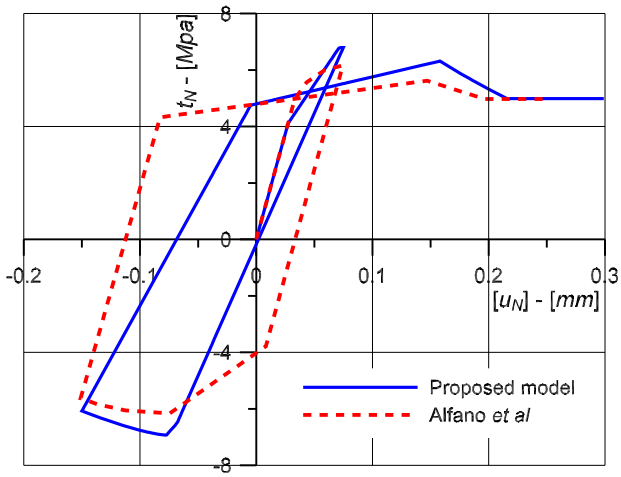

Fig. 13. Models comparison in a cyclic loading path.

of a step by step approximated resolution strategy, which requires time-discretization of loading path. Each loading step, of the discretized non-linear structural problem, is solved by a Newton-Raphson scheme, which consists in an iterative sequence of a predictor phase and of a corrector one, up to convergence. In the present work, the predictor phase is performed by means of a continuum tangent operator. Details of it are reported in Appendix. The corrector phase is solved by an Euler backward difference scheme.

In order to validate the proposed constitutive model, numerical simulation of an experimental test, reported in Magenes and Calvi (1997), is executed. In Magenes and Calvi (1997), the authors have led an extensive experimental research campaign on the behaviour of unreinforced brick masonry walls, performing several cyclic shear tests on walls with different aspect ratio and different axial load level. These tests have been made on two-wythes thick (English bond, 250 mm) walls with length of 1.0 m and height of 1.35 or 2.0 m. The walls have been subjected to constant compressive axial loads ($p = 0.6$ MPa, $p = 1.0$ MPa, $p = 1.2$ MPa) and to a cyclic tangential load, imposed by keeping the top and the bottom sections parallel, under control of the displacement horizontal component of the top section. Among several data, the experimental test, chosen in order to verify the effectiveness of FEM implementation, is the one conduced on the lowest wall ($h = 1.35$ m) subjected to the axial load $p = 0.6$ MPa. In fact, the failure mechanism, shown in this test, is mainly characterized by diagonal cracking with joint rupture and by negligible brick failure and, therefore, it appears to be the most suitable to validate the proposed interface constitutive model.

Fig. 14a shows the masonry wall arrangement and Fig. 14b shows a mesh detail. The wall bricks are discretized by eight nodes finite elements with linear elastic behaviour. The constitutive parameters adopted for the analysis are collected in Table 2.

The cyclic load is applied in terms of imposed displacement at the wall top section, whose horizontal degree of freedoms are restrained. Moreover, in order to keep horizontal the wall top section, a multifreedom constrain condition has been applied to relevant vertical degree of freedoms, by a master-slave approach, and the overall constant vertical load has been applied to the master degree of freedom.

The time history of the horizontal displacement, imposed at the top section, is reported in Fig. 15, which shows that an increasing sequence of repeated loading cycles is assumed.

Fig. 16 plots numerical and experimental responses to the first five cycles of loading path, in which the structure exhibits its maximum carrying capacity, in terms of horizontal displacement *vs* horizontal force applied at the top section. A quite good agreement between the numerical results and the experimental data can be observed. In fact, the simulation is able to catch accurately the peak load level of each load cycle and the wall stiffness reduction, whereas it underestimates residual displacements and hysteretic dissipation. The numerical structural response to the subsequent load cycles exhibits a constant peak load and, as shown in Fig. 17, it is not able to catch the progressive reduction of the load carrying capacity observed in the experimental data. Finally, the numerical simulation stops due to lack of convergence. In Figs. 18 and 19 tangential stress distributions are, respectively, plotted at time $t = 12.0$ s and 25.0 s, with reference to the relevant wall deformed configurations.

Table 2
Parameters adopted for masonry brick wall analyses.

Brick wall	Young modulus	E	2200 MPa
	Poisson ratio	ν	0.15
Interface sound fraction	Normal elastic stiffness	K_N^s	2000N/mm^2
	Tangential elastic stiffness	K_T^s	2000N/mm^2
Cracked fraction	Normal elastic stiffness	K_N^c	2000N/mm^2
	Tangential elastic stiffness	K_T^c	20N/mm^2
	Frictional coefficient	α	0.7
	Dilatancy coefficient	β	0.3639
	Normal displacement elastic limit	$\bar{u}_e$	7.010^{-5}mm
	Normal displacement crack limit	$\bar{u}_f$	7.510^{-1}mm
	Dilatancy limit displacement	$\bar{\delta}$	0.5 mm

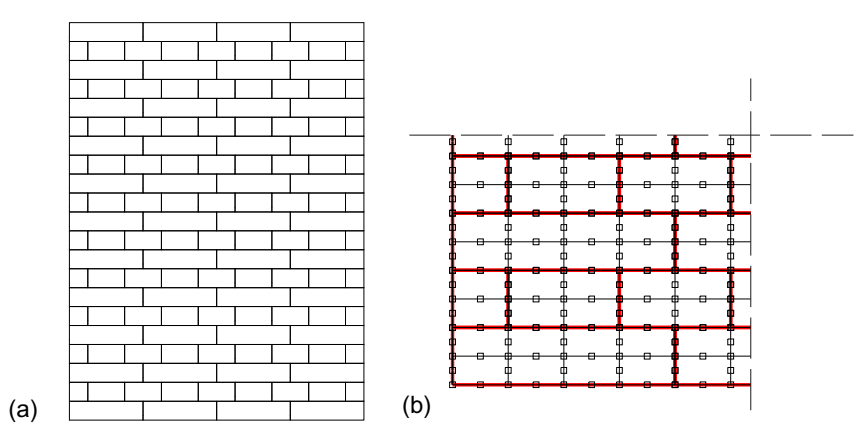

Fig. 14. (a) Masonry brick wall arrangement. (b)Bricks and joints mesh detail.

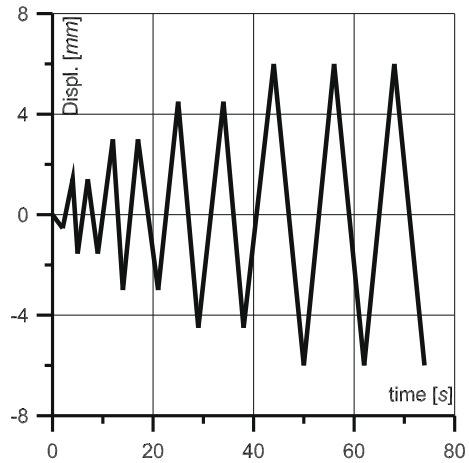

Fig. 15. Imposed horizontal displacement history.

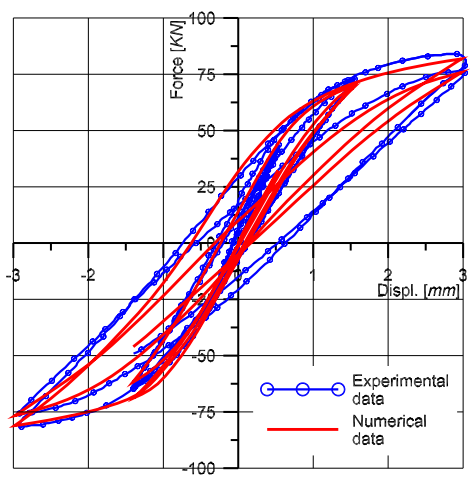

Fig. 16. Structural response to the first five loading cycles.

5. Conclusions

The proposed interface model appears to be able to catch, over the initial elastic behaviour, the damaging mechanism of the initially sound adhesive material and the pure frictional behaviour of the fully cracked one. The transition between the sound state and the fully cracked one, developed in a thermodynamically consistent framework, is governed by the interface damage variable, which measures the pointwise microcracked fraction, in which the frictional behaviour acts, and the sound fraction, where the behaviour is still elastic.

In the present paper it has been highlighted that the elastic stiffness parameters of cracked fraction have to be smaller than the relevant sound fraction ones, in order to ensure a positive dissipation during damaging process. The latter aspect may represent an improvement with respect to similar existing models, based on the same mesoscale interpretation of the damage variable as in (Alfano and Sacco, 2006). Moreover, if the elastic parameters of the two fractions are equal, the damage mechanism does not produce any stiffness degradation.

The proposed model is able to reproduce opening-reclosing mechanisms of the fully cracked material, thanks to a specific kinematic state vector variable, which represents the pointwise detachment between the cracked interface edges with zero tensile tractions. This behaviour is not adequately caught by means of plasticity based models, which simulate the fully cracked interface opening by plastic deformation development and, in the re-closing step, immediately enter the compressive phase; it means that the opening relative displacement does not represent a physical detachment between the cracked interface edges, but only a plastic deformation which can not vanish.

In the proposed formulation the contact problem between the interface edges, under compressive traction, is modeled by penalty method, which is an approximated approach classically used in interface modeling. As limit, this approximated approach causes compenetration between interface edges. Furthermore, when the limit value of dilatancy deformation is reached, a sharp behaviour change can produce convergence troubles in the nonlinear analysis.

The proposed modeling approach is suitable to some further enrichment. Namely: a higher order damage hardening law; a gradual reduction law for dilatancy phenomenon, instead of the cut off condition of Eq. (35), in order to avoid possible lack of convergence problems; finally, a softening law in the frictional plasticity, which allows to model asperities smoothing and breaking phenomena, in order to reproduce the carrying capacity reduction observed at the last stage of the experimental test.

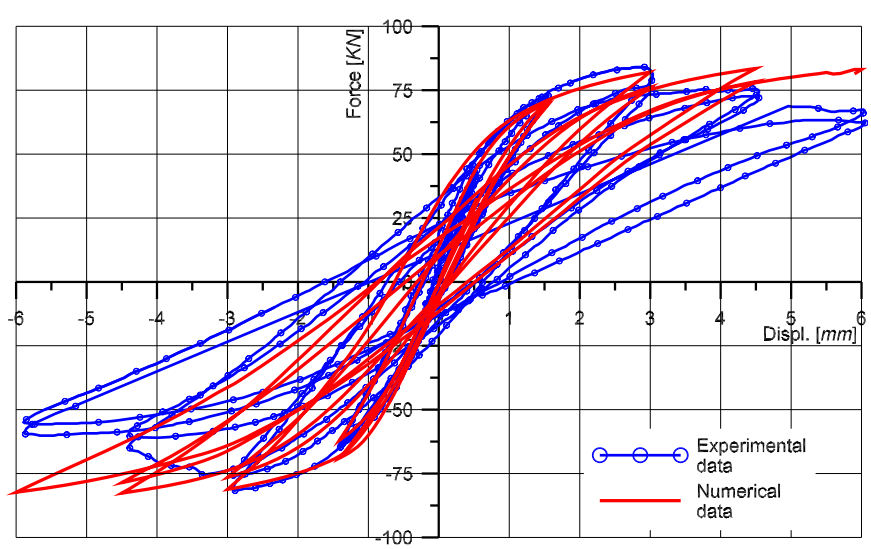

Fig. 17. Structural response to the entire loading path.

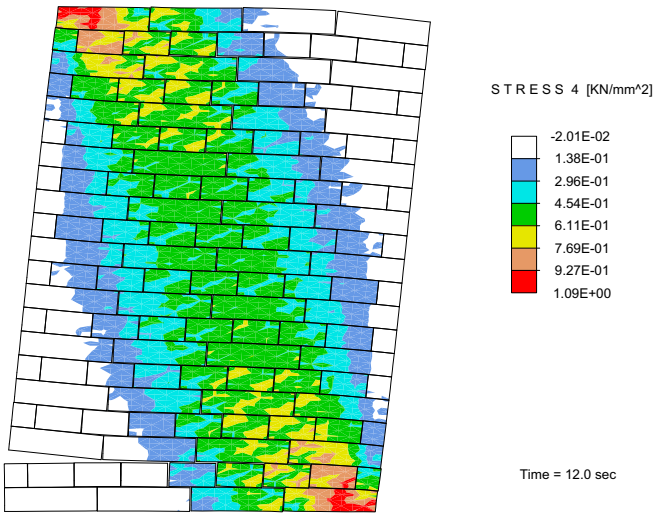

Fig. 18. Tangential stress distribution at time $t = 12.0\,s$.

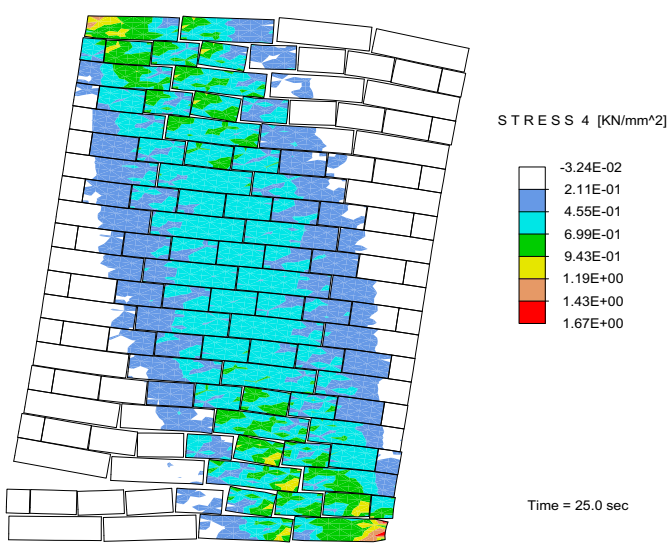

Fig. 19. Tangential stress distribution at time $t = 25.0\,s$.

Appendix A. Continuum tangent operator

The incremental constitutive laws can be effectively written using the continuum tangent operator, which is

$$\mathbf{K}^t = \frac{\partial \mathbf{t}}{\partial [\![\mathbf{u}]\!]} + \frac{\partial \mathbf{t}}{\partial \omega}\left(\frac{\partial \omega}{\partial [\![\mathbf{u}]\!]}\right)^T + \frac{\partial \mathbf{t}}{\partial \boldsymbol{\delta}_c^p}\left(\frac{\partial \boldsymbol{\delta}_c^p}{\partial [\![\mathbf{u}]\!]}\right)^T, \tag{39}$$

where $\mathbf{t}$ is defined in Eq. (19). The continuum tangent operator has to be defined with reference to four different conditions: elastic state ($\phi_d < 0$ and $\phi_p < 0$), damage activation state ($\phi_d = 0$ and $\phi_p < 0$), plasticity activation state ($\phi_d < 0$ and $\phi_p = 0$) and damage-plasticity activation state ($\phi_d = 0$ and $\phi_p = 0$).

A.1. Elastic state

The following trivial relation holds

$$\mathbf{K}_{el}^t = \frac{\partial \mathbf{t}}{\partial [\![\mathbf{u}]\!]} = \begin{bmatrix} (1-\omega)K_N^s + \omega K_N^c H(-\delta_{cN}^e) & 0 \\ 0 & (1-\omega)K_T^s + \omega K_T^c H(-\delta_{cN}^e) \end{bmatrix}. \tag{40}$$

A.2. Damage activation state

In increasing damage condition, the following loading relation holds

$$\dot{\phi}_d = \dot{Y} - \dot{\chi} = 0 \tag{41}$$

which, considering that $\dot{\boldsymbol{\delta}}_s^p = 0, \dot{\boldsymbol{\delta}}_c^p = 0$ and considering the rate form of Eqs. (4), (23) and (24), becomes

$$\dot{\phi}_d = (\mathbf{K}_s [\![\mathbf{u}]\!] - \mathbf{K}_c \boldsymbol{\delta}_c^e)^T [\![\dot{\mathbf{u}}]\!] - h\dot{\xi} = 0. \tag{42}$$

Where $h = d\chi/d\xi$ is a damage hardening modulus. On the basis of Eq. (29), the damage multiplier is given

$$\dot{\lambda}_d = \dot{\xi} = \dot{\omega} = \frac{1}{h}(\mathbf{K}_s [\![\mathbf{u}]\!] - \mathbf{K}_c \boldsymbol{\delta}_c^e)^T [\![\dot{\mathbf{u}}]\!]. \tag{43}$$

The traction–displacement relation of Eq. (19), in rate form, becomes

$$\dot{\mathbf{t}} = (1-\omega)\mathbf{K}_s [\![\dot{\mathbf{u}}]\!] + \omega \mathbf{K}_c [\![\dot{\mathbf{u}}]\!] - \dot{\omega}(\mathbf{K}_s [\![\mathbf{u}]\!] - \mathbf{K}_c \boldsymbol{\delta}_c^e) \tag{44}$$

and, *in virtue* of the following relation

$$\dot{\mathbf{t}} = \left[\frac{\partial \mathbf{t}}{\partial [\![\mathbf{u}]\!]} + \frac{\partial \mathbf{t}}{\partial \omega}\left(\frac{\partial \omega}{\partial [\![\mathbf{u}]\!]}\right)^T\right][\![\dot{\mathbf{u}}]\!] \tag{45}$$

the symmetric continuum tangent operator reads

$$\mathbf{K}^t = \frac{\partial \mathbf{t}}{\partial [\![\mathbf{u}]\!]} + \frac{\partial \mathbf{t}}{\partial \omega}\left(\frac{\partial \omega}{\partial [\![\mathbf{u}]\!]}\right)^T = \mathbf{K}_{el}^t - \mathbf{K}_{dm}^t \tag{46}$$

where

$$\mathbf{K}_{dm}^t = \frac{1}{h}(\mathbf{K}_s [\![\mathbf{u}]\!] - \mathbf{K}_c \boldsymbol{\delta}_c^e)(\mathbf{K}_s [\![\mathbf{u}]\!] - \mathbf{K}_c \boldsymbol{\delta}_c^e)^T. \tag{47}$$

A.3. Plasticity activation state

In increasing plastic strain condition ($\dot{\omega} = 0$), the following plastic loading relation holds

$$\dot{\phi}_p = \left[\frac{\partial \phi_p}{\partial \mathbf{t}_c}\right]^T \dot{\mathbf{t}}_c = 0 \tag{48}$$

where, considering Eqs. (18) and (34), it follows that

$$\dot{\mathbf{t}}_c = \omega \mathbf{K}_c \left([\![\dot{\mathbf{u}}]\!] - \frac{\partial \Omega_p}{\partial \mathbf{t}_c}\dot{\lambda}_p\right) \tag{49}$$

with

$$\frac{\partial \Omega_p}{\partial \mathbf{t}_c} = \begin{bmatrix} \beta \\ \mathrm{sgn}(t_{cT}) \end{bmatrix}, \qquad \frac{\partial \phi_p}{\partial \mathbf{t}_c} = \begin{bmatrix} \alpha \\ \mathrm{sgn}(t_{cT}) \end{bmatrix}. \tag{50}$$

Considering Eqs. (49), (48) becomes

$$\dot{\phi}_p = \omega \left[\frac{\partial \phi_p}{\partial \mathbf{t}_c}\right]^T \mathbf{K}_c \left([\![\dot{\mathbf{u}}]\!] - \frac{\partial \Omega_p}{\partial \mathbf{t}_c}\dot{\lambda}_p\right) = 0 \tag{51}$$

and the plasticity multiplier is given

$$\begin{aligned} \dot{\lambda}_p &= \left[\frac{\partial \phi_p}{\partial \mathbf{t}_c}\right]^T \mathbf{K}_c [\![\dot{\mathbf{u}}]\!] \Big/ \left[\frac{\partial \phi_p}{\partial \mathbf{t}_c}\right]^T \mathbf{K}_c \frac{\partial \Omega_p}{\partial \mathbf{t}_c} \\ &= [\alpha K_N^c; \mathrm{sgn}(t_{cT}) K_T^c][\![\dot{\mathbf{u}}]\!] / (K_T^c + \alpha\beta K_N^c). \end{aligned} \tag{52}$$

Considering Eq. (45), the unsymmetric continuum tangent operator reads

$$\begin{aligned} \mathbf{K}^t &= \frac{\partial \mathbf{t}}{\partial [\![\mathbf{u}]\!]} + \frac{\partial \mathbf{t}}{\partial \boldsymbol{\delta}_c^p}\left(\frac{\partial \boldsymbol{\delta}_c^p}{\partial [\![\mathbf{u}]\!]}\right)^T = (1-\omega)\mathbf{K}_s + \omega \mathbf{K}_c - \omega \mathbf{K}_c \frac{\partial \Omega_p}{\partial \mathbf{t}_c}\dot{\lambda}_p \\ &= \mathbf{K}_{el}^t - \mathbf{K}_{pl}^t \end{aligned} \tag{53}$$

where after some algebra

$$\mathbf{K}^t_{pl} = \frac{\omega}{K^c_T + \alpha\beta K^c_N}\begin{bmatrix}\beta K^c_N \\ K^c_T \mathrm{sgn}(t_{cT})\end{bmatrix}\left[\alpha K^c_N; \quad K^c_T \mathrm{sgn}(t_{cT})\right]. \tag{54}$$

A.4. Damage-plasticity activation state

In condition of increasing plastic strain and increasing damage, the following loading relations hold

$$\dot{\phi}_d = \dot{Y} - h\dot{\xi} = 0 \tag{55}$$

$$\dot{\phi}_p = \left(\frac{\partial \phi_p}{\partial \mathbf{t}_c}\right)^T \dot{\mathbf{t}}_c = 0 \tag{56}$$

where

$$\dot{Y} = [\![\mathbf{u}]\!]^T \mathbf{K}_s [\![\dot{\mathbf{u}}]\!] - \boldsymbol{\delta}^{eT}_c \mathbf{K}_c ([\![\dot{\mathbf{u}}]\!] - \dot{\boldsymbol{\delta}}^p_c). \tag{57}$$

By means of substitution of Eqs. (57) and (34) in Eqs. (55) and (56), plastic multiplier of Eq. (52) is obtained, whereas the damage multiplier is

$$\dot{\lambda}_d = \dot{\omega} = \dot{\xi} = \frac{1}{h}\left[[\![\mathbf{u}]\!]^T \mathbf{K}_s [\![\dot{\mathbf{u}}]\!] - \boldsymbol{\delta}^{eT}_c \mathbf{K}_c \left([\![\dot{\mathbf{u}}]\!] - \frac{\partial \Omega_p}{\partial \mathbf{t}_c}\dot{\lambda}_p\right)\right] \tag{58}$$

which gives

$$\begin{aligned}\dot{\omega} = {} & ([\![\mathbf{u}]\!]^T \mathbf{K}_s - \boldsymbol{\delta}^{eT}_c \mathbf{K}_c)[\![\dot{\mathbf{u}}]\!] + \frac{1}{h(K^c_T + \alpha\beta K^c_N)} \boldsymbol{\delta}^{eT}_c \mathbf{K}_c \frac{\partial \Omega_p}{\partial \mathbf{t}_c} \\ & \times \left[\alpha K^c_N; \quad \mathrm{sgn}(t_{cT}) K^c_T\right][\![\dot{\mathbf{u}}]\!].\end{aligned} \tag{59}$$

The traction–displacement relation, in rate form, is

$$\dot{\mathbf{t}} = (1-\omega)\mathbf{K}_s [\![\dot{\mathbf{u}}]\!] + \omega \mathbf{K}_c \left([\![\dot{\mathbf{u}}]\!] - \frac{\partial \Omega_p}{\partial \mathbf{t}_c}\dot{\lambda}_p\right) - \dot{\omega}(\mathbf{K}_s [\![\mathbf{u}]\!] - \mathbf{K}_c \boldsymbol{\delta}^e_c) \tag{60}$$

and, after some algebra, the relevant unsymmetric continuum tangent operator is

$$\mathbf{K}^t = \mathbf{K}^t_{el} - \mathbf{K}^t_{pl} - \mathbf{K}^t_{dm} - \mathbf{K}^t_{dp} \tag{61}$$

where

$$\mathbf{K}^t_{dp} = \frac{1}{h(K^c_T + \alpha\beta K^c_N)}(\mathbf{K}_s [\![\mathbf{u}]\!] - \mathbf{K}_c \boldsymbol{\delta}^e_c)(\mathbf{K}_c \boldsymbol{\delta}^e_c)^T \frac{\partial \Omega_p}{\partial \mathbf{t}_c}\left[\alpha K^c_N; \quad \mathrm{sgn}(t_{cT}) K^c_T\right]. \tag{62}$$

In active plasticity condition, the symmetry requirement of continuum tangent operator is recovered assuming $\beta = \alpha$.

References

Alfano, G., Crisfield, M.A., 2001. Finite element interface models for the delamination analysis of laminated composites: mechanical and computational issues. I. Jour. Num. Meth. Eng. 50, 1701–1736.

Alfano, G., Marfia, S., Sacco, E., 2006. A cohesive damage-friction interface model accounting for water pressure on crack propagation. Comp. Meth. Appl. Mech. Eng. 196, 192–209.

Alfano, G., Sacco, E., 2006. Combining interface damage and friction in a cohesive-zone model. Int. J. Numer. Meth. Eng. 68, 542–582.

Allix, O., Blanchard, L., 2006. Mesomodeling of delamination: towards industrial applications. Compos. Sci. Technol. 66, 731–744.

Allix, O., Ladeveze, P., 1992. Interlaminar interface modeling for the prediction of delamination. Int. J. Compos. Struct. 22 (4), 235–242.

Bazant, Z.P., Oh, B.-H., 1983. Crack band theory for fracture of concrete. Mater. Struct. 16, 155–177.

Bazant, Z.P., Planas, J., 1998. Fracture and Size Effect in Concrete and Other Quasibrittle Materials. CRC Press, Boca Raton and London.

Carol, I., Lopez, C.M., Roa, O., 2001. Micromechanical analysis of quasi-brittle materials using fracture-based interface elements. Int. J. Numer. Meth. Engng. 52, 193–215.

Carpinteri, A., 1986. Mechanical Damage and Crack Growth in Concrete: Plastic Collapse to Brittle Fracture. Martinus Nijhoff Publishers, Dordrecht.

Cedolin, L., Dei Poli, S., Iori, I., 1987. Tensile Behavior of Concrete. J. Eng. Mech. Div., ASCE 113, 431–449.

Cocchetti, G., Maier, G., Shen, X.P., 2002. Piecewise linear models for interfaces and mixed mode cohesive cracks. CMES 3 (3), 279–298.

Corigliano, A., 1993. Formulation, identification and use of interface models in the numerical analysis of composite delamination. Int. J. Solids Struct. 30 (20), 2779–2811.

Gambarotta, L., 2004. Friction-damage coupled model for brittle materials. Eng. Fract. Mech. 71, 829–836.

Gambarotta, L., Lagomarsino, S., 1997. Damage models for the seismic response of brick masonry shear walls. Part I: the mortar joint model and its application. Earth. Eng. Str. Dyn. 26, 423–439.

Giambanco, G., Mroz, Z., 2001. The interphase model for the analysis of joints in rock masses and masonry structures. Meccanica 36, 111–130.

Gurtin, M.E., 1979. Thermodynamics and the cohesive zone in fracture. J. Appl. Math. Phys. 30, 991–1003.

Hillerborg, A., Modeer, M., Petersson, P.E., 1976. Analysis of crack formation and crack growth in concrete by means of fracture mechanics and finite elements. Cement Concrete Res. 6, 773–782.

Lemaitre, J., Chaboche, J.-L., 1990. Mechanics of Solids Materials. Cambridge University Press.

Liu, W.K., Hao, S., Belytschko, T., Li, S., Chang, C.T., 2000. Multi-scale methods. Int. J. Numer. Meth. Eng. 47, 1343–1361.

Magenes, G., Calvi, M., 1997. In-plane seismic response of brick masonry walls. Earth. Eng. Struct. Dyn. 26, 1091–1112.

Mi, Y., Crisfield, M.A., Davies, G.A.O., 1998. Progressive delamination using interface elements. J. Compos. Mater. 32 (14), 1246–1272.

Mortara, G., Boulon, M., Ghionna, V.N., 2002. A 2-D constitutive model for cyclic interface behaviour. Int. J. Num. Analyt. Meth. Geomech. 26, 1071–1096.

Oliveira, D.V., Lourenco, P.B., 2004. Implementation and validation of a constitutive model for the cyclic behaviour of interface element. Comput. Struct. 82, 1451–1461.

Point, N., Sacco, E., 1996. A delamination model for laminated composites. Int. J. Solids Struct. 33 (4), 483–509.

Qiu, Y., Crisfield, M.A., Alfano, G., 2001. An interface element formulation for the simulation of delamination with buckling. Eng. Fract. Mech. 68, 1755–1776.

Tvergaard, V., 1990. Effect of fiber debonding in a whisker-reinforced metal. Mater. Sci. Eng. 125, 203–213.

Zienkiewicz, O.C., Taylor, R.L., 2000. The finite element method, 5th ed. Butterworth–Heinemann Press.

Zou, Z., Reid, S.R., Li, S., 2003. A continuum damage model for delamination in laminated composites. Jur. Mech. Phys. Solids 51, 333–356.